

mixture of tetrol and 9-methoxy-BP 4,5-diol. It has been reported that the 9-hydroxy-BP 4,5-oxide is a metabolite responsible, at least in part, for the binding of BP to DNA in rat hepatocytes (9). It has not been possible to prepare this compound synthetically, and so its 9-methoxy analog has been used. The lowest singlet absorption spectra of the two compounds correspond to that of chrysene and are therefore very similar and blue-shifted relative to the absorption of tetrol. The conventional fluorescence spectra of tetrol, 9-hydroxy-BP 4,5-diol, and 9-methoxy-BP 4,5-diol are essentially identical with emission maxima at 380 and 400 nm. Since the lowest singlet absorption spectra of tetrol and BPDE-DNA are also very similar, the selectivity problem for the tetrol-4,5-diol binary mixture is equivalent to that for a mixture of the adducts of DNA formed with BPDE and 9-hydroxy-BP 4,5-oxide. The FLN spectra of the mixture are shown in Fig. 2. Because the absorption spectra of the two compounds are shifted relative to each other, they can be distinguished by selective excitation. One can see this selectivity by comparing the lower spectrum of Fig. 2 with the tetrol spectrum in Fig. 1. The upper spectrum of Fig. 2 is due entirely to 9-methoxy-BP 4,5-diol. Thus, it is established that, after the isolation of nucleic acids from cells exposed to BP, the BPDE and 9-hydroxy-BP 4,5-oxide adducts could be distinguished by FLN spectrometry. This is a considerable simplification over the best current method for this characterization, which involves extensive enzyme digestion of the DNA, derivitization, and high-performance liquid chromatographic (HPLC) analysis (10, 11).

Our results demonstrate that FLN spectra for highly substituted PAH derivatives bound to polymeric materials can be obtained and that fluorescence line narrowing in polar glasses is a promising approach for high-selectivity analysis of DNA obtained after in vivo exposure to PAH mixtures. Such analyses will require improvements in sensitivity, which are possible at this time (12).

VOLKER HEISIG
ALAN M. JEFFREY

Cancer Center/Institute for Cancer Research, Division of Environmental Science, and Department of Pharmacology, Columbia University, New York 10032

MICHAEL J. MCGLADE
GERALD J. SMALL

Ames Laboratory, Department of Energy, and Department of Chemistry, Iowa State University, Ames 50011

References and Notes

1. P. Daudel, M. Duquesne, P. Vigny, P. L. Grover, P. Sims, *FEBS Lett.* **57**, 250 (1975); V. Ivanovic, N. E. Geacintov, I. B. Weinstein, *Biochem. Biophys. Res. Commun.* **70**, 1172 (1976).
2. J. C. Brown, J. A. Duncanson, Jr., G. J. Small, *Anal. Chem.* **52**, 1711 (1980).
3. I. Chiang, J. M. Hayes, G. J. Small, *ibid.* **54**, 315 (1982); J. M. Hayes, I. Chiang, M. J. McGlade, J. A. Warren, G. J. Small, *Soc. Photo-Opt. Instrum. Eng. J.* **286**, 117 (1981); J. H. Eberly, W. C. McColgin, K. Kawaoka, A. P. Marchetti, *Nature (London)* **251**, 215 (1974).
4. Y. Yang, A. P. D'Silva, V. A. Fassel, *Anal. Chem.* **53**, 894 (1981).
5. R. I. Personov, in *Spectroscopy and Excitation of Condensed Molecular Systems*, V. M. Agronovich and R. M. Hochstrasser, Eds. (North-Holland, New York, 1983), chap. 10.
6. H. V. Gelboin, *Physiol. Rev.* **60**, 1107 (1980).
7. A. M. Jeffrey *et al.*, *Nature (London)* **269**, 348 (1977); *J. Am. Chem. Soc.* **98**, 5714 (1976).
8. J. C. Brown, thesis, Iowa State University (1982).
9. B. Jernstrom, S. Orrenius, O. Undeman, A. Groslund, A. Ehrenberg, *Cancer Res.* **38**, 2600 (1978).
10. V. Heisig, R. Santella, C. Cortez, R. G. Harvey, A. M. Jeffrey, *Proc. Am. Assoc. Cancer Res.* **24**, 68 (1983).
11. K. W. Jennette *et al.*, *Biochemistry* **16**, 932 (1977).
12. M. J. McGlade, thesis, Iowa State University (1983).
13. H. Brown, A. M. Jeffrey, I. B. Weinstein, *Cancer Res.* **39**, 1673 (1979).
14. Supported by National Cancer Institute grant CA 021111 and Department of Energy contract W-7405-eng-82, Office of Health and Environmental Research.

26 August 1983; accepted 22 November 1983

External Imaging of Cerebral Muscarinic Acetylcholine Receptors

Abstract. A radioiodinated ligand that binds to muscarinic acetylcholine receptors was shown to distribute in the brain by a receptor-mediated process. With single-photon-emission imaging techniques, radioactivity was detected in the cerebrum but not in the cerebellum, whereas with a flow-limited radiotracer, radioactivity was detected in cerebrum and cerebellum. Single-photon-emission computed tomography showed good definition of the caudate putamen and cortex in man.

The muscarinic acetylcholine receptor (m-AChR) appears to play an essential role in many physiological and behavioral responses (1). Sleep, avoidance behavior, learning, and memory are thought to be mediated by m-AChR. A decrease in m-AChR density has been observed in elderly patients, those with

Huntington's chorea, and those with Alzheimer's dementia. Ethanol, barbiturates, and antidepressants as well as chronic exposure to insecticides, may also affect the concentration of the m-AChR (2, 3). Most of these observations have been made in autopsy studies in humans or in animal studies. None of

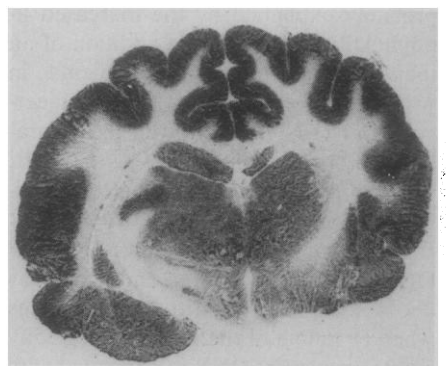
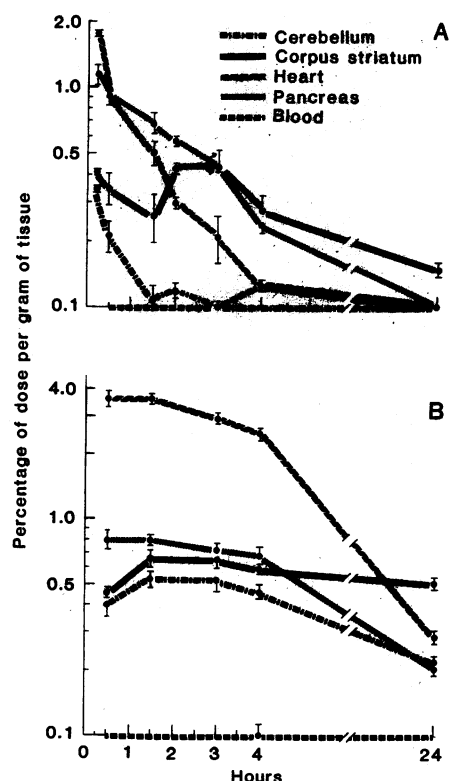
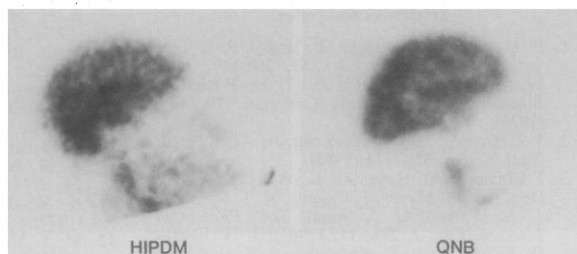


Fig. 1 (left). (A) Distribution of (R)-4-[¹²⁵I]IQNB in Sprague-Dawley rats as a function of time after femoral vein injection. (B) Distribution of (R)-[³H]IQNB in Sprague-Dawley rats as a function of time after femoral vein injection. The average value and the standard error for six rats are shown at each time point. Fig. 2 (right). Autoradiograph of (R)-4-[¹²⁵I]IQNB in a cat 15 minutes after injection. Results after 2 hours were similar. Coronal section, 20 μm thick; 500 μCi of the radioiodinated material was injected intravenously under light anesthesia (Innovar); the animal was killed by barbiturate injection and frozen (Freon and dry ice); and the brain was embedded in carboxymethyl cellulose. Exposure time, 10 days on SB5 film.

Fig. 3. Lateral Anger camera images of the head after injection of the perfusion agent, [^{123}I]HIPDM (left), and (*R*)-4-[^{123}I]QNB (right). On the perfusion image, uptake is seen in both the cortex and cerebellum. On the (*R*)-4-[^{123}I]QNB image, uptake is seen in the cortex but not in the cerebellum. For the (*R*)-4-[^{123}I]QNB study, 4.9 mCi was injected intravenously in one of us.



these relationships has been observed in intact humans by external detection with receptor-specific radiotracers.

Recently (*R*)-3-quinuclidinyl-4-iodobenzilate [(*R*)-4-IQNB] (4) has been prepared with ^{125}I or with ^{123}I (5). The product is a mixture of two diastereomers because of the unresolved chiral center in the acid moiety. However, preliminary studies show that this is not the critical center because the affinity constants do not differ by more than a factor of 4, whereas the affinities of the (*R*)-3-quinuclidinyl derivative [(*R*)-QNB] and the (*S*)-3-quinuclidinyl derivative differ by a factor of 100. We have studied the distribution of (*R*)-4-IQNB in rats (Fig. 1); ^3H -labeled (*R*)-QNB was used as a control. The distribution of the two radiotracers is qualitatively similar, but the lung accumulation is greater for (*R*)-4-IQNB than for (*R*)-QNB. As a result, the concentration of ^{125}I was lower than the concentration of ^3H in target organs such as cerebrum and heart. This preferential lung accumulation of (*R*)-4-IQNB is probably explained by the increased lipophilicity caused by the addition of an iodine atom. Earlier experiments in which 50 nmole of (*RS*)-QNB was injected with (*R*)-4-IQNB showed the saturability of the binding sites of 4-IQNB, supporting the hypothesis that the distribution is primarily receptor-mediated (6). In addition, we showed that (*R*)-[^3H]-QNB binding in rat brain and heart was decreased compared with control values when 50 nmole of the pharmacologically active isomer (*R*)-QNB was injected with (*R*)-[^3H]QNB but was not decreased when the inactive isomer (*S*)-QNB was used (6). This stereoselective competition adds further support to a receptor-mediated mechanism of localization in vivo. These tests of saturability cannot be used in humans because of the high drug doses required and the associated toxicity with large doses.

In a cat (Fig. 2) and a dog (not shown) treated with (*R*)-4-[^{123}I]QNB we observed radioactivity in the cerebrum but not in the cerebellum. The concentration of m-AChR was not determined in the

cat, but in the dog the concentration is 474 pmole per gram of protein in caudate nucleus, 147 in the thalamus, 57 in the hypothalamus, and 36 in the cerebellar cortex (7).

Using planar emission imaging techniques, we compared the distribution of (*R*)-4-[^{123}I]QNB with the distribution of the flow-mediated agent [^{123}I]HIPDM (8) in a human subject (Fig. 3). These data show that HIPDM accumulates in both the cerebrum and cerebellum, as would be expected for a flow agent, but that (*R*)-4-[^{123}I]QNB accumulates only in the cerebrum. These observations suggest that the uptake of (*R*)-4-[^{123}I]QNB is receptor-mediated in the human because muscarinic receptors are at relatively low concentration in the cerebellum. Single-photon-emission computed

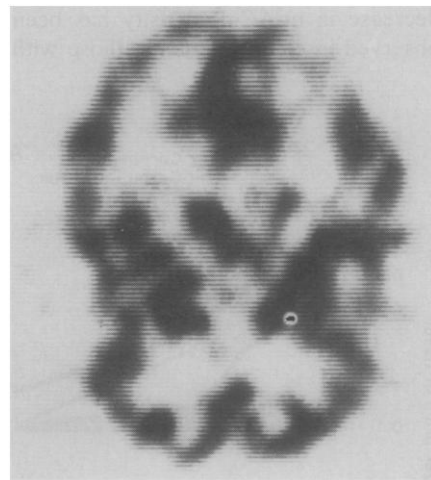


Fig. 4. A single tomographic slice obtained parallel to the orbital medial line through the region of the basal ganglia. The study was performed on one of us 20 minutes after injection of 4.9 mCi of 4-[^{123}I]QNB. The images were obtained in 20 minutes on the Harvard Multidetector Brain Scanning System, collecting 1,331,000 counts. The system resolution is 10 mm full width at half maximum with a slice thickness of 9.8 mm. The image shows increased uptake in the area of the caudate putamen having a high m-AChR concentration. Activity conforming to the convolutions of the gyral architecture of the cerebral cortex is visualized; more centrally, in the area of white matter and ventricles, no activity is seen.

tomography with a commercial ring system showed good definition of the caudate putamen area and the cerebral cortex in the human (Fig. 4). The concentration of a m-AChR in the human is 950 pmole per gram of protein in the caudate, 707 in the putamen, and 15 in the cerebellar hemisphere, as determined by Wastek and Yamamura (9). Enna *et al.* (10) determined that the concentration is 480 pmole per gram of protein in the caudate and 472 in the putamen but could not detect m-AChR in the cerebellum. Nordström *et al.* (11) determined that the cerebral cortex of untreated patients contained 500 pmole per gram of protein. Only the cerebrum was detected when (*R*)-4-[^{123}I]QNB was used in a human subject (Fig. 3). If the values of Enna *et al.* (10) are the correct ones, then the high ratio of radioactivity in the caudate putamen to radioactivity in the cerebellum in images of dog, cat, and man is understandable. The receptor concentration in the rat can be obtained only by use of a pharmacokinetic model (12). However, in dog, cat, and man the receptor concentration appears to determine the distribution of radioactivity. These data indicate that receptor-binding radiotracers can be used in humans to visualize m-AChR by external imaging.

WILLIAM C. ECKELMAN*

RICHARD C. REBA

WACLAW J. RZESZOTARSKI

RAYMOND E. GIBSON

George Washington University Medical Center, Washington, D.C. 20037

THOMAS HILL

New England Deaconess Hospital, Boston, Massachusetts 02215

B. LEONARD HOLMAN

Brigham and Women's Hospital, Boston, Massachusetts 02115

THOMAS BUDINGER

University of California, Berkeley 94720

JAMES J. CONKLIN

ROBERT ENG

MICHAEL P. GRISSOM

Armed Forces Radiobiology Research Institute, Bethesda, Maryland 20014

References and Notes

1. R. W. Olsten, T. D. Reisine, H. I. Yamamura, *Life Sci.* **27**, 801 (1980).
2. G. D. Tollefson, S. E. Senogles, W. H. Frey II, V. B. Tuason, S. E. Nicol, *Biol. Psychiatry* **17**, 555 (1982).
3. L. G. Costa, B. W. Schwab, S. D. Murphy, *Biochem. Pharmacol.* **31**, 3407 (1982).
4. (*R*)-(-)-3-quinuclidinyl-(*RS*)- α -hydroxy- α -(4-iodophenyl)phenylacetate.
5. W. J. Rzeszotarski *et al.*, *J. Med. Chem.*, in press.
6. W. C. Eckelman *et al.*, *J. Pharm. Sci.*, in press.
7. C. R. Hiley and A. S. V. Burgen, *J. Neurochem.* **22**, 159 (1974).
8. HIPDM is *N,N,N'*-trimethyl-*N'*-[2-hydroxy-3-methyl-5-iodobenzyl]-1,3-propanediamine [H. F. Kung, K. M. Trampusch, M. Blau, *J. Nucl. Med.* **24**, 66 (1983)].

9. G. J. Wastek and H. I. Yamamura, *Mol. Pharmacol.* **14**, 768 (1978).
 10. S. J. Enna *et al.*, *J. Neurochem.* **28**, 233 (1977).
 11. O. Nordström, A. Westlind, A. Uden, B. Meyerson, C. Sachs, T. Barfai, *Brain Res.* **234**, 287 (1982).
 12. With (R)-[³H]QNB, the ratio of radioactivity in striatum to radioactivity in cerebellum (S/R) in rat is approximately 1.2:1 in vivo 2 hours after injection, whereas in vitro with isolated tissue, the S/R is 12:1 (603:51 measured in picomoles per gram of protein) in homogenized rat brain (13). With (R)-[¹²⁵I]QNB, we observed an increased S/R but this is due to an increased off rate in the cerebellum (14) (Fig. 1). The concentration of radioactivity in the striatum and cerebellum at each time point is a complex function of blood flow, rate constants, and receptor concentration.
 13. R. M. Kobayashi *et al.*, *Brain Res.* **154**, 13 (1978).
 14. R. E. Gibson, D. J. Weckstein, E. M. Jagoda, W. J. Rzeszotarski, R. C. Reba, W. C. Eckelman, *J. Nucl. Med.*, in press.
 15. We thank B. Moyer for production of the autoradiograph (Fig. 2). This work was supported by DOE contract AS05 82 ER60039.
- * Present address: Department of Nuclear Medicine, National Institutes of Health, Bethesda, Md. 20205.

20 September 1983; accepted 22 November 1983

Neuromagnetic Evidence of Spatially Distributed Sources Underlying Epileptiform Spikes in the Human Brain

Abstract. *Neuromagnetic measurements were performed on 17 subjects with focal seizure disorders. In all of the subjects, the interictal spike in the scalp electroencephalogram was associated with an orderly extracranial magnetic field pattern. In eight of these subjects, multiple current sources underlay the magnetic spike complex. The multiple sources within a given subject displayed a fixed chronological sequence of discharge, demonstrating a high degree of spatial and temporal organization within the interictal focus.*

Human epilepsy is a disorder characterized by an uncontrolled discharge of brain neurons that produces seizures. In focal epilepsy, the source of the seizure is confined to limited regions of the brain. In the interictal period between seizures, isolated electrical spikes may often be recorded both from the scalp and from electrodes implanted within the brain (1). Interictal spikes have aroused clinical interest because of the possible role that they may play in diagnosis and in identifying the epileptic focus for surgical resection. Interictal spikes are also of neurophysiological interest in that they represent the spontaneous activity of epileptogenic cortex in which the normal regulatory mechanisms have been disrupted.

Examination of the precise timing of the interictal spike recorded simultaneously from a number of scalp locations in the electroencephalogram (EEG) indicates that these spikes frequently differ in wave shape and latency at different sites; thus, the recorded discharge often appears to be composed of separately firing generators within the epileptic zone (2). The impression of multiple generators is confirmed by recordings obtained from indwelling electrodes (3). Furthermore, when spike complexes recorded from such depth electrodes are averaged, evidence of a systematic temporal order of discharge in adjacent cortical regions is often observed (4). Such data suggest the presence of preferred pathways of epileptiform discharge within the region of the interictal focus, but are insufficient to provide a complete mapping of the discharge zone.

Interictal spikes recorded in the EEG also produce extracranial magnetic fields that may be recorded in the magnetoencephalogram (MEG) (5, 6). We demonstrated earlier that neuromagnetic mapping may identify the three-dimensional location of single sources of interictal spiking in the human brain with greater accuracy than the EEG (6), presumably because magnetic fields are not distorted or attenuated by the highly resistive skull (7). We now report that complex patterns of multifocal interictal discharges may be mapped directly from measurements of extracranial magnetic fields to provide a clear visualization of the contributing generators. These patterns exhibit a high degree of temporal and spatial organization of discharges within the epileptic zone.

Subjects were drawn from an ongoing neuromagnetic study of the interictal spike complex and consisted of 17 patients with focal (partial) seizure disorders. All subjects displayed orderly magnetic fields associated with interictal spiking. In nine subjects, the interictal spike appeared to originate from a single source. However, in the other eight subjects, distinct spatiotemporal discharge patterns suggested multiple intracranial generators. Two of these subjects showed particularly evident separation in the timing and location of sources producing the discharge sequence. Both had frequent interictal EEG spikes localized in the right temporal region.

The normal component of the extracranial magnetic field produced by spontaneous interictal spikes was measured and mapped with previously developed

procedures (6, 8). Visually identified interictal spikes in the scalp EEG recorded from a bitemporal bipolar montage (9) were used as time markers to generate digital averages of the magnetic signal over at least 20 spikes for each MEG probe position in a rectangular recording matrix covering the interictal focus. Sequential magnetic field maps were computed at 4-msec intervals during the averaged magnetic spike complex. From these, distinct temporal components of the magnetic spike were identified. The three-dimensional locations of putative sources were calculated for the identified magnetic field maxima of each component (10). These field distributions were plotted on the photographic image of each subject's head. Finally, computerized tomographic scans (CT) were obtained at levels indicated by the surface MEG localization to determine the position and depth of underlying cortical structures.

Figure 1A displays an outline of the right side of the first subject's head, with both the MEG recording matrix (dots) and scalp EEG electrode locations marked. The routine scalp EEG obtained with bipolar recording (Fig. 1E) showed a focal right anterior-midtemporal spike (electrodes F8-T4) which was used as a time marker for averaging ten channels of referential EEG (Fig. 1F) (11). The EEG spike from different regions of the right hemisphere occurred with a slight variation in latency.

Averaged magnetic spikes measured from each point in the MEG recording matrix are shown in Fig. 1G. Two distinct spike morphologies may be observed in areas of the matrix labeled a and b. Each of these spike morphologies appears in opposite polarity within a complementary region of the matrix (labeled a and b). Superimposed traces of the complementary pairs (solid and dotted lines in Fig. 1B) indicate that they are nearly mirror images, reflecting scalp locations where the magnetic flux simultaneously emerge from (upward deflection) and reenter (downward deflection) the cranium. Such a magnetic field pattern is expected if the underlying source for each of the pairs is modeled as a current dipole oriented tangentially to the scalp (12). The measured fields therefore provide evidence of two dipoles or sources (a and b) that differ in both location and orientation.

The discharge sequence between the two sources is composed of four components. The magnetic fields associated with each component (Fig. 1, H to K) display well-defined maxima where the normal components of the magnetic flux